2015-03

Energetic And Topological Insights Into The Supramolecular Structure Of Dicationic Ionic Liquids

UTD AUTHOR(S): Izabelle M. Gindri

Frizzo, C. P., C. R. Bender, A. Z. Tier, I. M. Gindri, et al. 2015. "Energetic and topological insights into the supramolecular structure of dicationic ionic liquids." Crystengcomm 17(15): 2996-3004.

CrystEngComm

PAPER

View Article Online
View Journal | View Issue

Cite this: *CrystEngComm*, 2015, **17**, 2996

Energetic and topological insights into the supramolecular structure of dicationic ionic liquids†

C. P. Frizzo,*[a] C. R. Bender,[a] A. Z. Tier,[a] I. M. Gindri,[b] P. R. S. Salbego,[a] A. R. Meyer[a] and M. A. P. Martins*[a]

Received 12th January 2015,
Accepted 2nd March 2015

DOI: 10.1039/c5ce00073d

www.rsc.org/crystengcomm

The crystal structures of dicationic ILs [DBMIM][2BF$_4$] (**1**) and [DBMIM][2Br]·[2H$_2$O] (**2**) were investigated in order to explore the intermolecular interactions in these compounds. An energetic and topological approach for characterization of supramolecular clusters in organic crystals was used. The study of the crystals was done by considering the stabilization energy and topological properties such as contact surfaces and energy content between cations and neighboring anions (supramolecular clusters). The study showed that: **1** is auto-organized into layers (one-dimensional structure) by an anion–cation interaction (weak electrostatic and ionic), and the three-dimensional supramolecular structure of **2** is constructed through simultaneous interactions between cations, anions, and water molecules. This network results in interaction chains in two different directions. Additionally, the supramolecular cluster approach allowed evaluation of the participation of the topological component during the formation of the crystals of **1** and **2**. Among the different types of interactions proposed, the most predominant was the one classified as type III, which has small and medium energy values, and a medium-sized contact surface. The thermal and morphological properties were also studied to further characterize these materials and to better understand the resulting structure–property relationships.

Introduction

The ultimate goal of crystal engineering is to control intermolecular interactions during the crystallization process in order to build solid-state materials with desired properties.[1] To accomplish this goal, it is necessary to understand the environment of intermolecular interactions and their role in directing one-, two-, and three-dimensional assemblies. Better comprehension of intermolecular interactions allows crystal structures to be correlated with material properties, which may be used as a powerful tool in the rationalization of new materials.[2] The crystal design of organic materials is receiving much attention from researchers in different fields, including crystallography, theoretical chemistry, nanotechnology, crystal engineering, and pharmaceutical science. Studies have shown that there is great potential for revealing the detailed intermolecular interactions in crystal structures. Synchrony among the aforementioned disciplines will be essential for the evolution in the determination of energetic and topological factors associated with these interactions.

Recently, we proposed a new energetic and topological approach for the characterization of the crystallization process in organic compounds.[3] According to this approach, the crystal should be analyzed as a supramolecular cluster formed by a central molecule and its first molecular coordination sphere. The supramolecular cluster is considered to be the smallest portion of the crystal that contains all the interactions of the crystal. In other words, it is the portion that provides all the necessary information for understanding the intermolecular interactions of the entire crystal. In this model, which considers the contact surface and energetic content between the molecules of the supramolecular cluster, intermolecular interactions can be classified into four types, according to the energy and surface distribution. The crystalline structures evaluated in this study consist of a series of neutral organic compounds with different electronic and topological characteristics; however, the crystals of charged organic molecules were not investigated. In this context, ionic liquid (IL) emerges as an interesting charged molecule model, given its electronic structure and range of potential applications.[4] In particular, dication-containing ILs are a

[a] *Núcleo de Química de Hetrociclos (NUQUIMHE), Department of Chemistry, Federal University of Santa Maria, Brazil. E-mail: clarissa.frizzo@gmail.com, mmartins@base.ufsm.br*

[b] *Department of Bioengineering, University of Texas at Dallas, Richardson, USA*

† Electronic supplementary information (ESI) available: Figures obtained from Diamond – crystal and molecular structure visualization software, PVD by TOPOS, calculation details, thermograms and simulated X-ray powder diffraction patterns are given. CCDC 1028628. For ESI and crystallographic data in CIF or other electronic format see DOI: 10.1039/c5ce00073d

class of materials with growing use; for example, as liquid crystals,[5] metal coating catalysts[6] in organic reactions,[7,8] high temperature lubricants and fluids for heat transfer in materials science.[9,10] Despite the fact that the number of dicationic ILs mentioned in the literature is increasing, the relationship between supramolecular solid-state structures and their physicochemical characteristics is not yet well understood.[11–13] The solid-state structure has contributed to clarifying the microstructure of ILs and especially to understanding of ion-pair interactions and analysis of the local forces acting on individual molecules within an IL.[14] It has been suggested that these intermolecular forces are one of the molecular features which determine the properties of ILs.[15,16]

The purpose of this work is to validate the supramolecular approach for charged organic molecules, by using the single crystal structure of [DBMIM][BF_4] (**1**) and [DBMIM][2Br]·[2H_2O] (**2**)[13] — see Fig. 1. Another objective of this work is to establish relationships between the organization in the solid state (crystallization and growth ability) and the hydrophobicity of ILs in relation to anions Br^- and BF_4^-.

Results and discussion

Crystal structure and stability of 1 and 2

A single crystal of **1** was grown through acetone evaporation at room temperature, which resulted in colourless crystals with sizes of 0.57 × 0.43 × 0.36 mm^3. A single molecule of **2** was easily combined with water molecules, resulting in single crystals containing [DBMIM][2Br]·[2H_2O] molecules.[13] ORTEP views of **1** and **2**, with thermal ellipsoids at 50% probability, are shown in Fig. 2. The crystal structure of **1** is described here for the first time and all crystallographic and refinement data are listed in Table 1. Information on **2** can be found in the work of Tadesse *et al.*[13]

In order to better comprehend the crystalline structure of **1** and **2**, the intermolecular interactions of each IL will be discussed. In this discussion, interactions will be treated as polar and nonpolar. The packing of **1** demonstrated in Fig. 3 shows the influence of the amphiphilic feature of the cationic moiety. In the cation, there are both polar (imidazolium ring) and nonpolar fragments (alkyl chain), and the packing

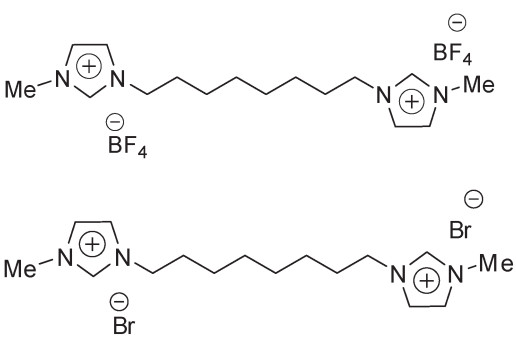

Fig. 1 Structures of dicationic ILs **1** and **2**.

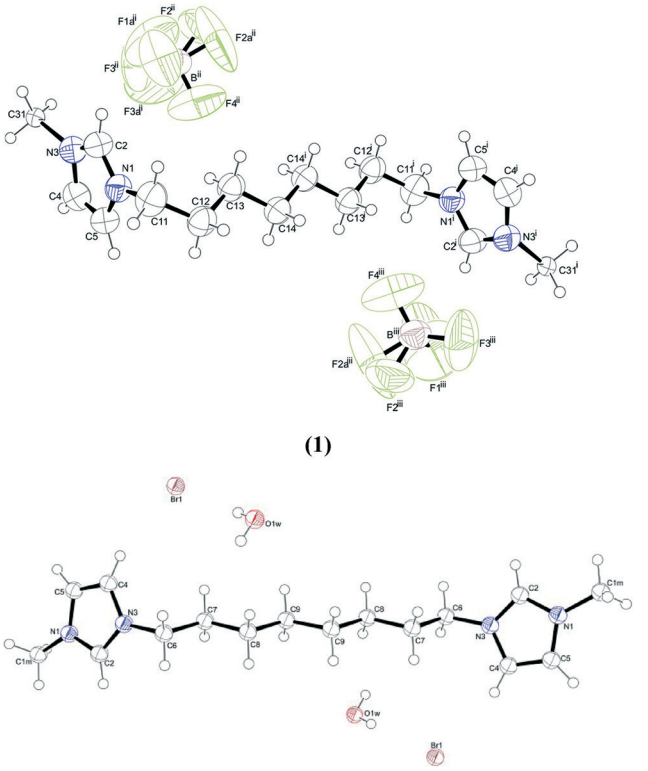

Fig. 2 ORTEP® 3 (ref. 17) for **1** and **2**, with thermal ellipsoids drawn at 50% probability level.

Table 1 Data collection and structure refinement for **1**

Compound	**1**
Empirical formula	$C_{16}H_{28}B_2F_8N_4$
Molecular weight	450.04
CCDC	1028628
Temperature (K)	293(2) K
Wavelength (Å)	0.71073
Crystal system	Monoclinic
Space group	$P2_1/c$
a (Å)	a = 5.4081(2)
b (Å)	b = 15.5202(8)
c (Å)	c = 13.3407(6)
α (degrees)	90
β (degrees)	100.649(2)
γ (degrees)	90
Volume ($Å^3$)	1100.46(9)
Z/density (calcd.) (mg m^{-3})	2/1.358
Absorption coefficient (mm^{-1})	0.128
F(000) (e)	468
Crystal size (mm)	0.57 × 0.43 × 0.36
θ Range for data collection (degrees)	2.03 to 27.19
Reflections collected/unique	29502/2421 [$R_{(int)}$ = 0.0243]
Completeness to θ = 27.19 (%)	99.4
Absorption correction	Gaussian
Max. and min. transmissions	0.9553 and 0.9305
Refinement method	Full-matrix least-squares on F^2
Data/restraints/parameters	2421/0/167
Goodness-of-fit on F^2	1.069
Final R indices [$I \geq 2\sigma(I)$]	R_1 = 0.0686, wR_2 = 0.2105
R indices (all data)[a]	R_1 = 0.0974, wR_2 = 0.2401
Largest diff. peak and hole (e $Å^{-3}$)	0.340 and −0.334

[a] $R_1 = \sum||F_o| - |F_c||/\sum|F_o|$, $wR_2 = \{\sum w(F_o^2 - F_c^2)^2/\sum[w(F_o^2)^2]\}^{1/2}$.

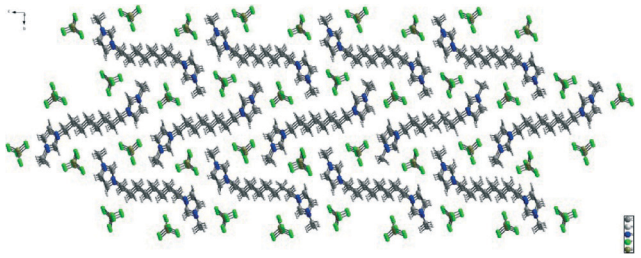

Fig. 3 Supramolecular structure of **1** using Diamond – crystal and molecular structure visualization software.[18]

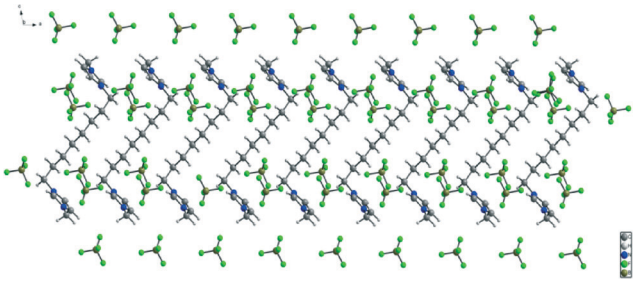

Fig. 4 Representation of the layer arrangement of **1**.

patterns exhibit both polar and nonpolar domains. The interactions in the polar domains can be assigned to ionic interactions and hydrogen bonds. In these polar domains it is observed that each imidazolium ring is surrounded by six anions, and each anion is surrounded by six imidazolium cations. The most predominant intermolecular interactions are ionic and hydrogen bonds of the H-imidazolium ring with an anionic fluorine atom. It must be mentioned that there are also significant hydrogen bonds between the hydrogen of the methyl and methylene substituents in the imidazolium ring, and the fluorine atom of the anions.

Otherwise or on the other hand, in the nonpolar domain, van der Waals contacts exist between the alkyl chains, as can be seen in Fig. 3. The three-dimensional arrangement of the imidazolium cations is formed by the stacking of alkyl chains through van der Waals interactions.

This feature is important in the field of materials science, where ILs have found potential use in film formation on metal surfaces. Also, performance in uses such as lubricants seems to depend on this kind of arrangement on metallic surfaces.[19] Another important nonpolar interaction occurs between methyl groups (linked to imidazolium rings) and alkyl chains, which also contributes to the zig-zag type of crystalline packing (Fig. 3). Thus, this molecular arrangement generates channels in which the tetrafluoroborate anions and imidazolium cations are accommodated as intercalated chains (Fig. 4). The crystal structure of **2** has already been published,[13] however, what we are proposing in this paper has yet to be addressed in great depth. Thus, in this paper we will take an approach that allows observations that have not been made up until now, despite knowing the crystal structure of this IL. The fact that **2** was crystallized in hydrate form ($\cdot 2H_2O$) resulted in greater complexity of the crystal structure in terms of intermolecular interactions, allowing polar intermolecular interactions between bromide, water, and the imidazolium ring. Each bromide interacts with at least two imidazolium cations and two water molecules *via* hydrogen bonds. In the cationic moiety, the interactions between the hydrogen of the imidazolium ring and bromide link the dication along the *c* axis, as shown in Fig. S5 (ESI†).

On the other hand, each water molecule interacts with two bromides and with three imidazolium rings (at different sites), as can be seen in Fig. 5. The interactions with bromine and two cations are *via* hydrogen bonds. The interaction between the water molecule and the third cationic moiety occurs *via* a lone pair–π (lp$\cdots\pi$) interaction, in which the pair of electrons from oxygen acts as a donor to the electron-deficient imidazolium ring. This kind of interaction is well documented between water, oxygen, and aromatic rings in studies involving proteins, and it appears to be essential for the stabilization of biological macromolecules.[20,21]

Besides the amphiphilic characteristic of the dications, the crystal packing of **2** does not show nonpolar domains. However, it is possible to observe van der Waals contacts between nonpolar portions of dication molecules. The central cation interacts with four other cationic moieties through its alkyl chain. Two methylene groups of the central alkyl chain are in contact with the methyl group of the imidazolium cation of the surrounding molecules. The other two methylenes of the central alkyl chain are involved in a C–H$\cdots\pi$ interaction with the same imidazolium ring involved in the lp$\cdots\pi$ interaction with a water molecule. Fig. S2 in the ESI† helps to visualize these interactions. These interaction chains occur in two different directions and overlap each other, resulting in the supramolecular structure observed in Fig. 6.

In order to understand the stability of the crystal and the supramolecular arrangement of **1** and **2**, a supramolecular cluster was constructed. Fig. 7 shows a dicationic unit surrounded by twelve tetrafluoroborate anions, with a Molecular Coordination Number (MCN) of 12, in the crystalline structure of **1**; whereas Fig. 8 shows a dicationic unit surrounded by ten bromide anions and eight water molecules in the crystalline structure of **2**. The contact surface between the dication and each anion and/or water molecule surrounding it was investigated, as was its corresponding energetic

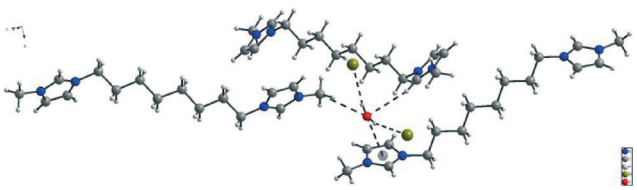

Fig. 5 Intermolecular interactions involving a water molecule in the crystalline structure of **2**, obtained *via* Diamond – crystal and molecular structure visualization software.[18]

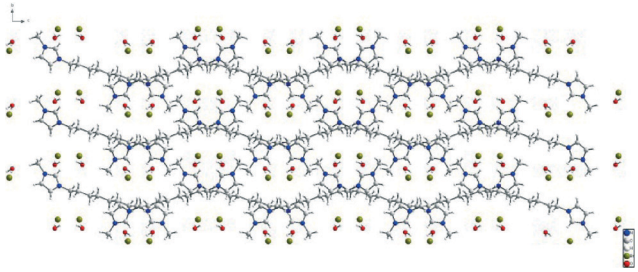

Fig. 6 Supramolecular structure of 2, obtained using Diamond – crystal and molecular structure visualization software.[18]

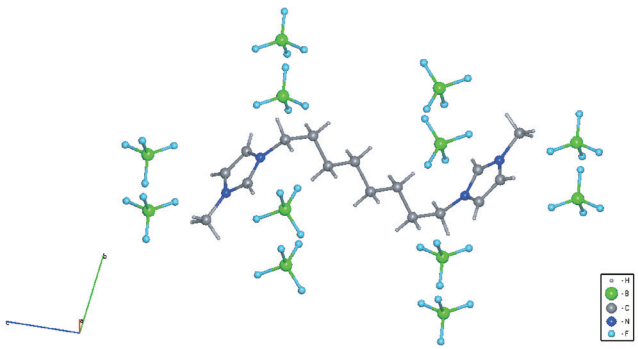

Fig. 7 Supramolecular cluster of 1 formed by a dicationic unit surrounded by 12 anions, constructed using TOPOS® 4.0 software.[27]

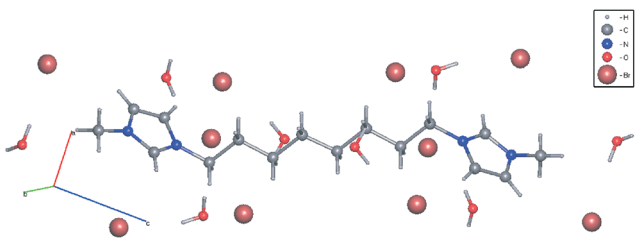

Fig. 8 Supramolecular cluster of 2 formed by a dicationic unit surrounded by 10 anions and 8 water molecules, constructed using TOPOS® 4.0 software.[27]

content. The contact surface between the cation and anions and/or water molecules was determined using the Voronoi–Dirichlet Polyhedron (VDP)[22–26] (see Fig. S3 and S4 in the ESI†).

To determine the energetic content of the interactions between the dication and each anion of the crystal structures of 1 and 2, density functional theory with empirical dispersion correction (DFT-D) was used. This method is routinely used for structure and energetic analyses of weakly-bonded systems.[28–31] The interaction energy ($G_{C1\cdots An}$) between the dication (C1) and each anion (An) is given by the difference in the energy of 1 ($E_{C1\cdots 2An}$) and the energy of 1 without an anion ($E_{C1\cdots An}$), less the energy of an isolated anion (E_{An}), as described in eqn (1). The schematic representation of the species involved in the calculation of the interaction energy between the dication (C1) and each anion (An) is given in Fig. S5 in the ESI.† The same logic was used to determine the energetic content of the interaction between 2 and each water molecule (see Fig. S5 in the ESI†).

$$G_{C1\cdots An} = (E_{C1\cdots 2An} - E_{C1\cdots An}) - E_{An} \quad (1)$$

Data from the contact surface ($C_{C1\cdots An}$) and the energy ($G_{C1\cdots An}$) between the dication and anions of 1 and 2 are listed in Table 2. As far as it is known, the correlation between the contact surface ($C_{C1\cdots An}$) and the energy ($G_{C1\cdots An}$) of the cation and anion of the ILs has not yet been determined. The relationship between $G_{C1\cdots An}$ (kcal mol^{-1}) and $C_{C1\cdots An}$ (Å^2) for 1 and 2 was determined, and the correlation coefficients were 0.77 for 1 and 0.46 for 2, suggesting that there is a poor correlation between the contact area and the contact energy between the cation and anion of ILs (see Fig. S6 in the ESI†).

Thus, in order to determine the relationship between the contact surface and the contact energy of the cation and anion, we hypothesize that the ratio between the $G_{C1\cdots An}$ and the $\sum G_{C1\cdots An}$ (sum of all cation–anion energies) for each anion, multiplied by the MCN (12 for 1 and 10 for 2) of each supramolecular cluster, could give us the distribution of energy per surface unit ($N_{GC1\cdots An}$).[3] The same rationale can be used for the ideal contribution of the surface contact ($NC_{C1\cdots An}$). The data calculated for 1 and 2 are given in Table 3 and show that all interactions make a similar contribution to the stabilization of the supramolecular cluster in terms of interaction energy and surface contact (type III). These results support our hypothesis that the supramolecular approach can be applied to charged molecules (anion–cation) such as ILs, in which ionic interactions predominate.

In a recent study involving neutral molecules, we showed that moieties such as NH_2 have great potential for introducing strong electrostatic interactions associated with a small contact surface.[3] Thus, we expected that the presence of water in the crystal packing of 1 could promote this kind of

Table 2 Surface contact[a] and interaction energy[b] between each anion and dication of ILs

	1		2	
C1⋯An	$G_{C1\cdots An}$ (kcal mol^{-1})	$C_{C1\cdots An}$ (Å^2)	$G_{C1\cdots An}$ (kcal mol^{-1})	$C_{C1\cdots An}$ (Å^2)
C1⋯A1	−71.74	12.41	−77.63	5.60
C1⋯A2	−74.64	17.29	−85.36	6.39
C1⋯A3	−76.58	13.24	−76.18	4.81
C1⋯A4	−79.61	20.84	−75.14	6.89
C1⋯A5	−69.72	15.71	−64.81	5.11
C1⋯A6	−66.08	9.72	−64.81	5.11
C1⋯A7	−69.72	15.71	−75.14	6.89
C1⋯A8	−66.08	9.72	−76.18	4.81
C1⋯A9	−76.58	13.24	−85.36	6.39
C1⋯A10	−79.61	20.84	−77.63	5.60
C1⋯A11	−71.74	12.41	—	—
C1⋯A12	−74.64	17.29	—	—

[a] Contact surface obtained using TOPOS®.[27] [b] Interaction energy obtained by Gaussian 09® (Theory level ω B97x-D/cc-pVDZ).[32]

Table 3 $NG_{C1\cdots An}$ and contact surface ($NC_{C1\cdots An}$) for ILs

	1		2	
C1···An	$NG_{C1\cdots An}$	$NC_{C1\cdots An}$	$NG_{C1\cdots An}$	$NC_{C1\cdots An}$
C1···A1	0.98	0.83	1.02	0.97
C1···A2	1.02	1.16	1.13	1.11
C1···A3	1.05	0.89	1.00	0.84
C1···A4	1.09	1.40	0,99	1.20
C1···A5	0.95	1.06	0.85	0.89
C1···A6	0.90	0.65	0.85	0.89
C1···A7	0.95	1.06	0.99	1.20
C1···A8	0.90	0.65	1.00	0.84
C1···A9	1.05	0.89	1.13	1.11
C1···A10	1.09	1.40	1.02	0.97
C1···A11	0.98	0.83	—	—
C1···A12	1.02	1.16	—	—

interaction. However, this was not observed in the crystal structure of 2. This result implies that the presence of an ionic intermolecular interaction probably prevents this kind of interaction and equalizes the energetic and surface contribution of each intermolecular interaction in the crystal stabilization. To better understand this result, the interaction energies of the cation, anion, and water of 2 (Table 4) were further investigated. The influence of water molecules on the energetic stabilization of crystal was confirmed through analysis of the interaction energy values obtained for interactions between 2 and water (Table 4). It was observed that the anions which have more energetic (stronger) intermolecular interactions with the dication have less energetic (weaker) intermolecular interactions with water. For example, in the C1···A4···H_2O7 system, the energy related to the A4···H_2O7 interaction is only −7 kcal mol^{-1}, while the energy of the C1···A4 interaction is −75 kcal mol^{-1} (Table 2, Fig. 9). On the other hand, considering the C1···A5···H_2O7 system, the A5···H_2O7 interaction energy is −26 kcal mol^{-1} (Table 4, Fig. 9), while the energy found for C1···A5 was −64 kcal mol^{-1}. Therefore, it is reasonable to think that the interaction energy of water with A4 and A5 involves compensation between the ionic (C1···An) and the hydrogen bond interactions (An···H_2O*n*) of the anions. The energy resulting from the interaction between the other anions of 2 and water was around −10 kcal mol^{-1}. The higher energy found between C1···A2 (−85 kcal mol^{-1} — see Table 2) was explained based on the existence of a stronger hydrogen bond between this anion and the acid hydrogen of the imidazolium ring of cation C1 (Table 2, Fig. 9).

In summary, it can be seen that A4 (yellow, Fig. 9) interacts strongly with C1 (−75.14 kcal mol^{-1}) and weakly with H_2O7 (−7.13 kcal mol^{-1}). Conversely, A5 (pink, Fig. 9) interacts weakly with C1 (−64.81 kcal mol^{-1}) and strongly with H_2O7 (−26.33 kcal mol^{-1}).

Table 4 Interaction energy and contact area for IL 2 and water

C1···An···H_2O*n*[a]	$G_{C1\cdots H_2O\cdots An}$[b] (kcal mol^{-1})	$C_{C1\cdots H_2O\cdots Na}$[c] (Å^2)
C1···A1···H_2O5	−10.13	12.82
C1···A10···H_2O6	−10.13	12.82
C1···A2···H_2O1	−11.07	18.42
C1···A9···H_2O4	−11.07	18.42
C1···A3···H_2O1	−10.34	17.68
C1···A8···H_2O4	−10.34	17.68
C1···A3···H_2O2	−13.96	20.36
C1···A8···H_2O3	−13.96	20.36
C1···A4···H_2O7	−7.13	17.41
C1···A7···H_2O8	−7.13	17.41
C1···A5···H_2O7	−26.33	16.67
C1···A6···H_2O8	−26.33	16.67

[a] Designation of the cation, anion and water molecules, in accordance with Fig. 2 and schematic in Fig. S5 (ESI). [b] Interaction energy obtained by Gaussian 09® (Theory level ω B97x-D/cc-pVDZ).[32] [c] Contact surface obtained using TOPOS®.[27]

Thermal characterization and the degree of amorphousness

Differential scanning calorimetry (DSC) analysis was performed for 1 and 2. For this study, samples of selected ILs were exposed to successive heating–cooling cycles. The results show that 1 and 2 have an amorphous (showing glass transition temperatures) and a crystalline percentage (exhibiting melting temperatures and crystallization). The thermal properties of 1 and 2 are described in Table 5, and DSC thermograms are depicted in the ESI† (Fig. S7 and S8).

The crystallinity percentage or the relative degree of the amorphous phase of 1 and 2 was determined from DSC data. The change in the heat capacity during the glass transition of the material can be used to measure the amorphous phase amount in the sample.[33] The molecular motion related to the glass transition is time dependent. Therefore, T_g and, consequently, the amorphous percentage, increase when the heating rate increases. From the amorphous percentage, the crystallinity percentage of the sample is estimated. The amorphization process of the samples was realized through heating and cooling cycles, using a heating rate between 2 °C min^{-1} and 17 °C min^{-1} for both ILs (1 and 2). The relative degree of amorphousness of 1 and 2 was determined using the ratio between the reverse heat capacity of the sample in the cycle with lower and higher heating rates. The ratio for 1 was 0.026 cal g^{-1} $°C^{-1}$/0.085 cal g^{-1} $°C^{-1}$ and for 2 it was 0.078 cal g^{-1} $°C^{-1}$/0.99 cal g^{-1} $°C^{-1}$. DSC thermograms of 1 and 2 at different heating rates are shown in the ESI† (Fig. S9 and S10).

From these results, it was possible to observe that 1 and 2 have a distinct crystalline content, because they progressively amorphized with the same thermal treatment and presented different degrees of amorphousness (56% and 78% for 1 and 2, respectively). From the amorphousness data, it is possible to deduce that the crystalline content of 1 and 2 are 44% and 22%, respectively. X-ray powder diffraction analysis (Fig. 10) of 1 shows thin, well defined, more intense peaks, indicating that the crystalline content of 1 is greater than that of 2.[34] Additionally, the comparison of the simulated spectra obtained through monocrystal diffraction data[35] (see Fig. S4 and S5 in the ESI†) supports the crystalline and amorphous

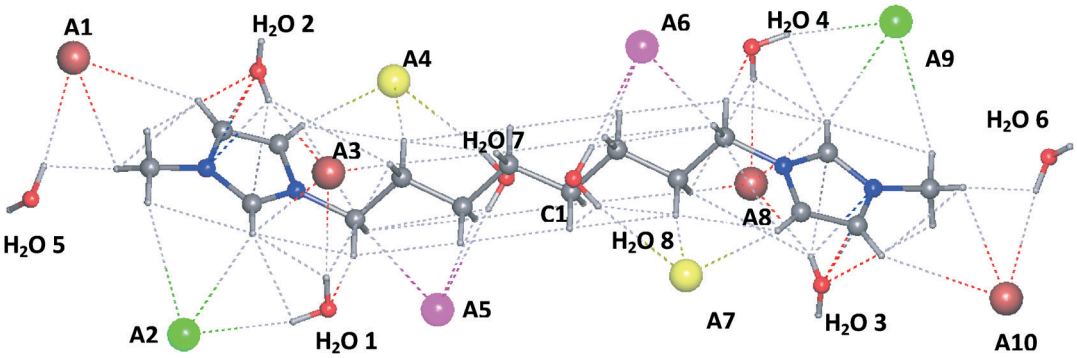

Fig. 9 Interactions between the dicationic unit of **2**, bromide anions, and water molecules, derived using TOPOS® 4.0 software.[27]

Table 5 Thermal properties of ILs

IL	T_g[a] (°C)	T_m[b] (°C)	ΔH_m[b] (kcal mol^{-1})	T_d[c] (°C)
1	−37.98 ± 0.13	69.55	6.91	453.61
2	−44.16 ± 0.39	69.58	8.45	326.83

[a] Glass transition temperature from the average of two cycles. [b] Data from first cycle. [c] Decomposition temperature.

contents of **1** and **2** that were found by calorimetric experiments. The SEM images of **1** and **2** also confirm the high crystalline content of **1** (Fig. 11). The image in Fig. 11a shows a typical crystal with well-defined morphological characteristics, whereas the image of **2** (Fig. 11b) shows that even at a higher approximation, the crystalline morphological characteristic is not well defined.

It is important to note that the X-ray powder diffraction spectra shown in Fig. 10, the SEM image shown in Fig. 11, and the thermal analysis of **2** were obtained using the compound synthesized in our laboratory. Thus, it is possible that this compound does not have exactly the same water content as the single crystal reported by Tadesse *et al.*[13] Thermogravimetric analysis (TGA) was carried out to determine the water content in **2**, which was found to be about 9% (see ESI,† Fig. S13).

Finally, the crystal packing efficiency (CPE) of each crystal was determined.[36] The CPE was 87% and 88% for **1** and **2**, respectively (see the ESI†). This result shows that despite **2** being crystallized with water, its CPE was not lower than **1**. In other words, the CPE is related to the crystalline content of each IL crystal and it shows that the crystalline content percentage of an IL does not indicate the packing efficiency. Additionally, the results show that it is reasonable to suggest that the water molecule in the crystal packing of **2** takes the place of anion units, because the crystal structure of **1** has twelve anion units surrounding one cationic unit, and the crystal structure of **2** has ten anions and eight water units surrounding one cationic unit.

General procedures

Materials. The reactants 1-methylimidazole, 1,8-dibromooctane, and sodium tetrafluoroborate were purchased from Sigma-Aldrich (USA) and the solvents were purchased from Tedia (Brazil). All chemicals have high-grade purity and were used without further purification.

Synthesis and characterization

The ILs were synthesized according to methodologies developed in our laboratories.[37,38] The IL structures were confirmed

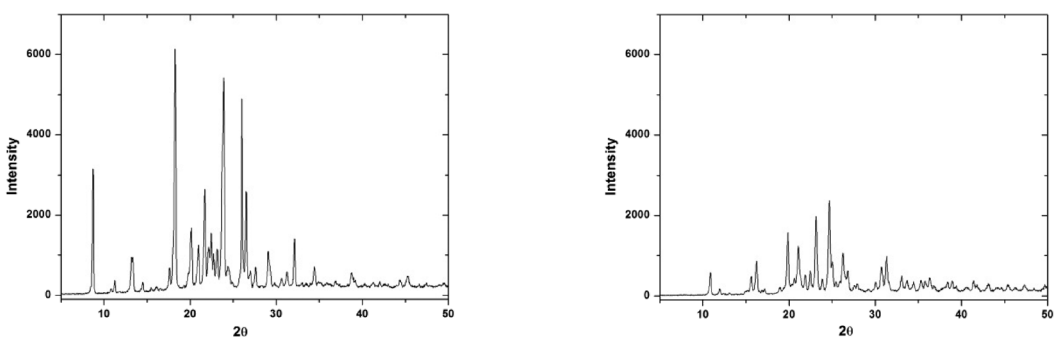

Fig. 10 X-ray powder diffraction patterns of (a) **1** and (b) **2**.[6]

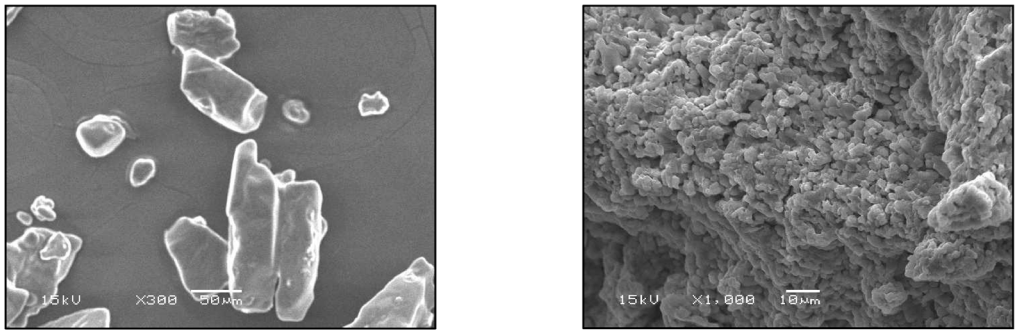

(a) (b)

Fig. 11 (a) SEM image of **1** at 50 μm and (b) SEM image of **2** at 10 μm.

using nuclear magnetic resonance (NMR) and mass spectrometry (MS). Electrospray ionization mass spectrometry (ESI-MS) analysis was performed with an Agilent Technologies 6460 Triple quadrupole 6460 (LC/MS-MS) (Agilent Technologies, USA), operating in positive-ion mode. The gas temperature was 300 °C, the flow rate of the drying gas was 5 L min^{-1}, and the nebulizer was set at 45 psi. The voltage of the capillary and the fragmentor was 3500 V and 0 V, respectively. The IL solutions in H_2O were introduced at a flow rate of 5 μl min^{-1}. Nitrogen was used as the nebulization gas and argon as the collision gas. Molecular ions were detected using positive mode, in which the m/z ratio is given for one dication and one anion. NMR ^1H and ^{13}C spectra were recorded using a Bruker DPX-200 (^1H at 200.13 MHz and ^{13}C at 50.32 MHz) and a Bruker DPX 400 (^1H at 400.13 MHz and ^{13}C at 100.32 MHz). The samples were prepared in 5 mm tubes at 298 K (digital resolution of ±0.01 ppm) in DMSO-d_6, using TMS as the internal reference or D_2O solutions. The NMR peak of D_2O (δ = 4.710) was used as the reference in determining the chemical shifts of ^1H in ILs. The data acquired are in accordance with the data reported in the literature for **1**[6] and **2**.[13]

Differential scanning calorimetry (DSC)

DSC experiments were performed using a MDSC Q2000 (T-zero™ DSC Technology, TA Instruments Inc., USA). Dry high purity (99.999%) nitrogen gas was used as the purge gas (50 mL min^{-1}). The instrument was initially calibrated in standard MDSC mode using the extrapolated onset temperatures of melting indium (156.60 °C) at a heating rate of 10 °C min^{-1}, and the heat from the fusion of indium (28.71 J g^{-1}). Heat capacity calibration was done by running standard sapphire (α-Al_2O_3) measurement at the experimental temperature. For the amorphousness study, a sample of both ILs ([DBMIM][2BF_4] and [DBMIM][2Br]·[2H_2O]) was subjected to one cycle of heating and cooling (−80 to 100 °C) for each heating rate used. The heating rates used were 2, 5, 7, 10, 12, 15 and 17 °C min^{-1} and gradually increased from lowest to the highest heating rate. The heating rate used for the melting point and glass transition determination of [DBMIM][2BF_4] and [DBMIM][2Br]·[2H_2O] was 10 °C min^{-1}. Samples were crimped in hermetic aluminum pans with lids. The sample mass was weighed on a Sartorius M 500 P to an accuracy of ±0.001 mg.

Thermogravimetric analysis (TGA)

TGA was performed on a TGA Q5000 (TA Instruments Inc., USA). The heating rate was 10 °C min^{-1} and the N_2 flow rate was 50 mL min^{-1}, ranging from 40 °C to 900 °C.

Scanning electron microscopy (SEM)

The morphology of **1** and **2** was examined with a field emission scanning electron microscope (SEM JEOL model JSM 6360 LV). The fractured samples were coated with gold for SEM analysis.

Powder X-Ray diffraction. The X-ray diffraction patterns were recorded on a Rigaku Miniflex 300 powder diffractometer (30 kV, 10 mA), connected to a Goniometer, with Cu Kα radiation (λ = 1.54051 Å). Patterns were collected in the step scan mode, with a step size of 0.03° and counting time of 0.9 s, in the scan range (2θ) from 5° to 50°. The powder was manually pressed inside the standard grooved sample holder. All spectra were collected in air at room temperature.

Crystallographic data collection and refinement

The diffraction measurements were performed on a Bruker SMART CCD diffractometer *via* graphite monochromatized Mo Kα radiation, with λ = 0.71073 Å.[39] The structures were solved by direct methods and refined by full-matrix least-squares on F^2, using the SHELXL package.[40] Absorption correction was done using the Gaussian method.[41] Anisotropic displacement parameters for non-hydrogen atoms were applied. The hydrogen atoms were placed at calculated positions with 0.96 Å (methyl CH_3), 0.97 Å (methylene CH_2), 0.98 Å (methyne CH), 0.93 Å (aromatic CH), and 0.82 Å (OH), using a riding model. Hydrogen isotropic thermal parameters were kept equal to $U_{iso}(H) = xU_{eq}$ (carrier C atom), with x = 1.5 for methyl groups, and x = 1.2 for other groups. The valence angles, C–C–H and H–C–H, of the methyl groups

were set to 109.5, and H atoms were allowed to rotate around the C–C bond.

Computational details

The intermolecular interaction energies between the cation and anion, and the anion and/or cation with water were determined for **1** and **2**, respectively, by single point calculations (without optimization of molecular geometry) performed with geometries obtained from X-ray diffraction. All quantum mechanical calculations were performed with the aid of the Gaussian 09 software package.[32] The energy calculations for the isolated anion (An), the cation/anion pair (C1···An), and the dication and two anions and water molecule (C1···An···H_2O*n*), which have been reported in this article, were performed using the DFT-D method with a ωB97x-D/cc-pVDZ basis set using the Gaussian 09 suite of programs.[32] The counterpoise method of Boys and Bernardi[42–45] was employed to minimize the basis set superposition error (BSSE). Considering the number of atoms in the molecules of **1** and **2**, the complexity of the calculations required, the computational cost, and the quality of results in some preliminary tests, we found that the level of calculation used in this study was fair.

Conclusion

The relationship between the contact surface and the contact energy for the cation–anion interaction of ILs was described for the first time and it was shown that all interactions contribute similarly to the stabilization of the supramolecular cluster. These results support the supramolecular cluster approach being used for charged organic molecules such as ILs. Furthermore, the determination of the energetic content of the interactions between the cations and anions (or water) in dicationic ILs showed a compensation between the ionic (C1···An) and hydrogen-bond interactions (An···H_2O*n*) of anions when water is in the crystal. This work also showed that the presence of water in the crystallized IL added complexity to the crystal structure, because the crystal structure of **1** is auto-organized into layers (one-dimensional structure) and **2** is constructed through simultaneous complex interactions between cations, anions, and water molecules *via* hydrogen bonds (three-dimensional supramolecular). The small size and hydrophobicity of the bromine anion in relation to tetrafluoroborate was probably the reason for its crystallization with water. Finally, the results corroborate with the potential uses of dicationic ILs, showing that their performance is dependent on their auto-assembly and crystalline properties, which change drastically according to the anion in the structure. For example, **1** has tetrafluorborate in its structure, which is more hydrophobic and tends to crystallize in double layers, something considered to be a positive feature in the lubricant field, for example. On the other hand, **2** is hygroscopic and tends to absorb water from the environment, indicating that it does have the double layer characteristic in the supramolecular structure, which may mean poor performance if used as a lubricant. These data were corroborated with thermal (DSC) and morphological data (XRD and SEM), which promoted the experimental crystal structure characterization and resulted in structure–property relationships, including the hydrophobicity of the anions and the crystalline content of the ILs in this study. These observations reinforce the anion's importance in the emergent properties of ILs.

Acknowledgements

The authors are grateful for the financial support of the National Council for Scientific and Technological Development (CNPq) — Universal/Proc. 474895/2013-0 and Universal/Proc. 475556/2012-7), the Foundation for Research Support of the State of Rio Grande do Sul (FAPERGS), and the Coordination for Improvement of Higher Education Personnel (CAPES/PROEX). The fellowships from CNPq (M.A.P.M., P. R. S. Salbego, I.M.G and C.R.B) and CAPES (A.Z.T. and A.R.M.) are also acknowledged.

Notes and references

1 G. R. Desiraju, *Crystal Engineering: The Design of Organic Solids*, Amsterdan, 54th edn, 1989, vol. 54.
2 C. M. Reddy, G. Rama Krishna and S. Ghosh, *CrystEngComm*, 2010, **12**, 2296.
3 M. A. P. Martins, C. P. Frizzo, A. C. L. Martins, A. Z. Tier, I. M. Gindri, A. R. Meyer, H. G. Bonacorso and N. Zanatta, *RSC Adv.*, 2014, **4**, 44337.
4 M. A. P. Martins, C. P. Frizzo, A. Z. Tier, D. N. Moreira, N. Zanatta and H. G. Bonacorso, *Chem. Rev.*, 2014, **114**, PR1.
5 L. Douce, J.-M. Suisse, D. Guillon and A. Taubert, *Liq. Cryst.*, 2011, **38**, 1653.
6 I. M. Gindri, C. P. Frizzo, C. R. Bender, A. Z. Tier, M. A. P. Martins, M. A. Villetti, G. Machado, L. C. Rodriguez and D. C. Rodrigues, *ACS Appl. Mater. Interfaces*, 2014, **6**, 11536.
7 Y. Q. Cai, Y. Lu, Y. Liu and G. H. Gao, *Catal. Lett.*, 2007, **119**, 154.
8 R. Wang, C. Jin, B. Twamley and J. M. Shreeve, *Inorg. Chem.*, 2006, **45**, 6396.
9 G. Yu, S. Yan, F. Zhou, X. Liu, W. Liu and Y. Liang, *Tribol. Lett.*, 2006, **25**, 197–205.
10 R. Ge, C. Hardacre, P. Nancarrow and D. W. Rooney, *J. Chem. Eng. Data*, 2007, **52**, 1819.
11 J. L. Anderson, R. Ding, A. Ellern and D. W. Armstrong, *J. Am. Chem. Soc.*, 2005, **127**, 593.
12 L. Leclercq and A. R. Schmitzer, *Cryst. Growth Des.*, 2011, **11**, 3828.
13 H. Tadesse, A. J. Blake, N. R. Champness, J. E. Warren, P. J. Rizkallah and P. Licence, *CrystEngComm*, 2012, **14**, 4886.
14 Y. Zhao, X. Hu, Q. Zhang and P. Guan, *Mater. Lett.*, 2010, **64**, 794.
15 K. Dong and S. Zhang, *Chemistry*, 2012, **18**, 2748.
16 K. Fumino, T. Peppel, M. Geppert-Rybczyńska, D. H. Zaitsau, J. K. Lehmann, S. P. Verevkin, M. Köckerling and R. Ludwig, *Phys. Chem. Chem. Phys.*, 2011, **13**, 14064.

17 L. J. Farrugia, ORTEP −3 for Windows - a version of ORTEP - III with a Graphical User Interface (GUI), *J. Appl. Crystallogr.*, 1997, **30**, 565.
18 *Diamond - Crystal and Molecular Structure Visualization Crystal Impact* - Dr. H. Putz & Dr. K. Brandenburg GbR, Kreuzherrenstr. 102, 53227 Bonn, Germany http://www.crystalimpact.com/diamond.
19 F. Zhou, Y. Liang and W. Liu, *Chem. Soc. Rev.*, 2009, **38**, 2590.
20 A. Jain, V. Ramanathan and R. Sankararamakrishnan, *Protein Sci.*, 2009, **18**, 595.
21 T. J. Mooibroek, P. Gamez and J. Reedijk, *CrystEngComm*, 2008, **10**, 1501.
22 T. G. Mitina and V. A. Blatov, *Cryst. Growth Des.*, 2013, **13**, 1655.
23 M. R. Singh, P. Verma, H. Tung, S. Bordawekar and D. Ramkrishna, *Cryst. Growth Des.*, 2013, **13**, 1390.
24 E. V. Peresypkina and V. A. Blatov, *Acta Crystallogr., Sect. B: Struct. Sci.*, 2000, **56**, 501.
25 V. A. Blatov, *Crystallogr. Rev.*, 2007, **10**, 249.
26 V. A. Blatov, L. V. Pogildyakova and V. N. Serezhkin, *Z. Kristallogr.*, 1998, **213**, 202.
27 *TOPOS® version 4.0 software*; V. A. Blatov and A. P. Shevchenko, Samara State University, Ac. Pavlov St., 443011 Samara, Russia; http://www.topos.ssu.samara.ru.
28 S. Grimme, *J. Comput. Chem.*, 2004, **25**, 1463–1473.
29 S. Grimme, J. Antony, S. Ehrlich and H. Krieg, *J. Chem. Phys.*, 2010, **132**, 154104.
30 P. Jurecka, J. Cerný, P. Hobza and D. R. Salahub, *J. Comput. Chem.*, 2007, **28**, 555.
31 J.-D. Chai and M. Head-Gordon, *Phys. Chem. Chem. Phys.*, 2008, **10**, 6615.
32 *Gaussian® version 09, Revision A.1*, M. J. Frisch, G. W. Trucks, H. B. Schlegel, G. E. Scuseria, M. A. Robb, J. R. Cheeseman, G. Scalmani, V. Barone, B. Mennucci, G. A. Petersson, H. Nakatsuji, M. Caricato, X. Li, H. P. Hratchian, A. F. Izmaylov, J. Bloino, G. Zheng, J. L. Sonnenberg, M. Hada, M. Ehara, K. Toyota, R. Fukuda, J. Hasegawa, M. Ishida, T. Nakajima, Y. Honda, O. Kitao, H. Nakai, T. Vreven, J. A. Montgomery, Jr., J. E. Peralta, F. Ogliaro, M. Bearpark, J. J. Heyd, E. Brothers, K. N. Kudin, V. N. Staroverov, R. Kobayashi, J. Normand, K. Raghavachari, A. Rendell, J. C. Burant, S. S. Iyengar, J. Tomasi, M. Cossi, N. Rega, J. M. Millam, M. Klene, J. E. Knox, J. B. Cross, V. Bakken, C. Adamo, J. Jaramillo, R. Gomperts, R. E. Stratmann, O. Yazyev, A. J. Austin, R. Cammi, C. Pomelli, J. W. Ochterski, R. L. Martin, K. Morokuma, V. G. Zakrzewski, G. A. Voth, P. Salvador, J. J. Dannenberg, S. Dapprich, A. D. Daniels, Ö. Farkas, J. B. Foresman, J. V. Ortiz, J. Cioslowski and D. J. Fox, Gaussian, Inc., Wallingford CT, 2009.
33 C. P. Frizzo, M. A. Villetti, A. Z. Tier, I. M. Gindri, L. Buriol, F. A. Rosa, R. M. Claramunt, D. Sanz and M. A. P. Martins, *Thermochim. Acta*, 2013, **574**, 63.
34 P. Varlashkin, *Am. Pharm. Rev.*, 2011, 14.
35 Mercury, Cambridge Crystallographic Data Centre 12 Union Road Cambridge CB2 1EZ, United Kingdom Web: http://beta-www.ccdc.cam.ac.uk Telephone: +44 1223 336408 Email: admin@ccdc.cam.ac.uk.
36 M. J. Turner, J. J. McKinnon, D. Jayatilaka and M. A. Spackman, *CrystEngComm*, 2011, **13**, 1804.
37 M. A. P. Martins, E. A. Guarda, C. P. Frizzo, E. Scapin, P. Beck, A. C. da Costa, N. Zanatta and H. G. Bonacorso, *J. Mol. Catal. A: Chem.*, 2007, **266**, 100.
38 M. A. P. Martins, E. A. Guarda, C. P. Frizzo, D. N. Moreira, M. R. B. Marzari, N. Zanatta and H. G. Bonacorso, *Catal. Lett.*, 2009, **130**, 93.
39 *Bruker, APEX2 (Version 2.1), COSMO (Version 1.56), BIS (Version 2.0.1.9) SAINT (Version 7.3A) and SADABS (Version 2004/1) and XPREP (Version 2005/4)*, Bruker AXS Inc., Madison, Wisconsin, USA, 2006.
40 G. M. Sheldrick, *Acta Crystallogr., Sect. A: Found. Crystallogr.*, 2008, **64**, 112.
41 P. Coppens, L. Leiserowitz and D. Rabinovich, *Acta Crystallogr.*, 1965, **18**, 1035.
42 S. F. Boys and F. Bernardi, *Mol. Phys.*, 1970, **19**, 553.
43 K. E. Riley and P. Hobza, *J. Phys. Chem. A*, 2007, **111**, 8257.
44 E. K. Riley, M. Pitonák, P. Jurecka and P. Hobza, *Chem. Rev.*, 2010, **110**, 5023.
45 K. E. Riley, J. A. Platts, J. Řezáč, P. Hobza and J. G. Hill, *J. Phys. Chem. A*, 2012, **116**, 4159.

